Non-opioid analgesia based on Gα signalling bias

Mark J. Wall[1*], Emily Hill[1], Robert Huckstepp[1], Giuseppe Deganutti[2], Michele Leuenberger[3], Barbara Preti[3], Kerry Barkan[4], Ian Winfield[4], Haifeng Wei[5], Wendy Imlach[6], Eve Dean[1], Cherise Hume[1], Stephanie Hayward[1], Jess Oliver[1], Fei-Yue Zhao[5], David Spanswick[5,6,7], Christopher A. Reynolds[2], Martin Lochner[3], Graham Ladds[4] and Bruno G. Frenguelli[1]

*Author for correspondence

[1]School of Life Sciences

University of Warwick

Gibbet Hill Rd

Coventry CV4 7AL, UK

[2]School of Biological Sciences

University of Essex

Wivenhoe Park

Colchester CO4 3SQ, UK

[3]Institute of Biochemistry and Molecular Medicine

University of Bern

3012 Bern, Switzerland

[4]Department of Pharmacology

University of Cambridge

Tennis Court Road

Cambridge CB2 1PD, UK

[5]NeuroSolutions Ltd, Coventry, UK.

[6]Department of Physiology

Monash Biomedicine Discovery Institute

Monash University

Innovation Walk

Clayton VIC 3800, Australia

[7]Warwick Medical School

University of Warwick

Gibbet Hill Rd

Coventry CV4 7AL, UK

Abstract

One third of all medicines act at G protein-coupled receptors (GPCRs). However, the identification of new therapeutic GPCR targets is limited by a fundamental property of GPCRs: their propensity to couple to different G protein alpha subunits (Gα) leading to multiple downstream cellular effects. This is especially the case for adenosine A_1 receptors (A_1Rs), the activation of which results in unwanted cardiorespiratory effects, severely limiting their clinical potential. We have discovered that the novel A_1R agonist, BnOCPA, unlike typical A_1R agonists, has a unique and highly selective Gα activation preference. Moreover, we found that BnOCPA is a potent and powerful analgesic without causing bradycardia, hypotension or respiratory depression. BnOCPA thus demonstrates a hitherto unknown Gα-selective activation of the native A_1R, sheds new light on the fundamentals of GPCR signalling, and reveals new possibilities for the development of novel therapeutics based on the far-reaching concept of biased agonism.

Abbreviated summary:

We describe the selective activation of an adenosine A_1 receptor-mediated intracellular pathway that provides potent analgesia in the absence of cardiorespiratory depression, paving the way for novel medicines based on the far-reaching concept of biased agonism.

Main text: G protein-coupled receptors (GPCRs) are the targets of many FDA-approved drugs (*1*). However, the promiscuity with which they couple to multiple intracellular signalling cascades leads to unwanted side effects, and limits both the range of GPCRs suitable for drug-targeting, and the number of conditions for which treatments could be developed (*2*). The four GPCRs for the purine nucleoside adenosine have particularly suffered as drug targets due to their promiscuous coupling, despite their potential for treating many pathological conditions including cancer, cardiovascular, neurological and inflammatory diseases (*3-5*). For example, activation of the widely-distributed adenosine A_1 receptor (A_1R) with currently available agonists elicits multiple actions in both the central nervous system (CNS), such as the inhibition of synaptic transmission and neuronal hyperpolarization, and in the cardiorespiratory system through slowing the heart (bradycardia), reducing blood pressure (hypotension) and affecting respiration (dyspnea) (*5-8*). These multiple effects severely limit the prospects of A_1R agonists as life-changing medicines, despite their potential in a wide range of clinical conditions including pain, epilepsy and cerebral ischemia (*5, 9-11*).

The therapeutic limitations of promiscuous GPCR coupling may be overcome through the development of biased agonists – compounds that selectively recruit one intracellular signalling cascade over another (*12, 13*). While this has most frequently been expressed in terms of Gα vs β-arrestin signalling (*14*), other forms of bias exist, including between individual Gα subunits (*12*). However, the challenge remains in translating Gα signalling bias observed *in vitro* to tangible, and physiologically-relevant, selectivity at native receptors *in vivo* (*2, 15*). Accordingly, while the potential to selectively drive the G protein coupling of A_1Rs has been described in several *in vitro* studies (*16-19*), to date no A_1R-specific agonist has been reported that can elicit Gα biased agonism at native A_1Rs in intact physiological systems. Achieving such an aim would highlight the fundamental importance of agonist bias in general, and moreover, specifically unlock the widespread clinical potential of A_1R agonists.

The novel A_1R agonist BnOCPA uniquely discriminates between pre- and postsynaptic actions of A_1Rs in the intact mammalian CNS.

The possibility that biased agonists exist for the native A_1Rs found in intact physiological systems was revealed during the CNS profiling of novel, potent and selective A_1R agonists we described previously (*20*). During these studies we identified one particular agonist, BnOCPA (Fig. 1A; compound 6 in ref (*20*)), which displayed properties that were not consistent with those of prototypical A_1R agonists such as adenosine, CPA and NECA. In accordance with the effects of standard A_1R agonists, BnOCPA potently inhibited excitatory synaptic transmission in rat hippocampal slices (Fig. 1B to F and fig. S1A to D), an effect attributable to activation of presynaptic A_1Rs on glutamatergic terminals (*7*) (Fig. 1B; fig. S1E, F). However, in stark contrast to adenosine and CPA, BnOCPA did not activate postsynaptic A_1Rs (Fig. 1B) to induce membrane hyperpolarisation, even at concentrations 15 times the IC_{50} for synaptic transmission (Fig. 1G, H).

Since there are no reported structural differences between pre- and postsynaptic A_1Rs that would prevent BnOCPA binding, we reasoned that, if BnOCPA bound to postsynaptic A_1Rs, but without efficacy, it might behave in a manner analogous to a receptor antagonist in preventing activation by other A_1R agonists, a property that has been predicted and observed for biased agonists at other receptors (*12*). To test this, we pre-applied BnOCPA then applied CPA (in the continued presence of BnOCPA). Remarkably, the co-application of CPA and BnOCPA resulted in a significant reduction of the effects of CPA on membrane potential (Fig. 1H; fig. S2A, B). In addition, membrane hyperpolarisation induced by the endogenous agonist adenosine was reversed by BnOCPA (fig. S2C). To test whether BnOCPA blocked K^+ channels mediating postsynaptic hyperpolarisation, or in some other way non-specifically interfered with G protein signalling, we applied the $GABA_B$ receptor agonist baclofen to CA1 pyramidal neurons. BnOCPA had no effect on membrane hyperpolarisation produced by baclofen (fig. S2D, E), confirming that the actions of BnOCPA were specific to the A_1R. These observations, of a lack of effect of BnOCPA on postsynaptic membrane potential, likely

explained why, in a model of seizure activity with prominent postsynaptic depolarisation that promotes neuronal firing, (low Mg^{2+}/high K^{+}), BnOCPA had little effect (Fig. 1I, J). In contrast, equivalent concentrations of CPA completely suppressed neuronal firing (Fig. 1I, J).

BnOCPA demonstrates unique Gα signalling bias.

To investigate the molecular basis for the unprecedented properties of BnOCPA, we generated a recombinant cell system (CHO-K1 cells) expressing the human A_1R (hA_1R). BnOCPA was a potent (IC_{50} 0.7 nM; Table 1) full agonist at the hA_1R and bound to the receptor with an affinity equal to that of CPA and NECA, and higher than that of adenosine (Fig. 2A, B; table S1). Using individual pertussis toxin (PTX)-insensitive variants of individual Gi/o subunits transfected into PTX-treated cells (*17, 20*) we observed that adenosine, CPA, NECA and the novel unbiased agonist HOCPA (*20*) coupled to a range of Gi/o subunits, and in particular Goa (Fig. 2C to E; Table 1; table S1; fig. S3 & S4). In stark contrast, BnOCPA had a distinctive and highly selective Gα subunit activation profile and discriminated between the two Go isoforms in being unable to activate Goa (Fig. 2C to E; Table 1; table S1; fig. S3, S5). We hypothesised that BnOCPA should therefore reduce the actions of adenosine on the inhibition of cAMP accumulation via Goa. This was indeed the case (Fig. 2F) and had parallels with the antagonising effects of BnOCPA on membrane potential in the CNS (Fig. 1G, H). We excluded the possibility that the actions of BnOCPA and the prototypical A_1R agonists were mediated via β-arrestins using a BRET assay for β-arrestin recruitment (fig. S6). We observed no β-arrestin recruitment at the A_1R using either BnOCPA, CPA or adenosine (fig. S6), observations that are consistent with those previously reported for A_1Rs (*21-25*). The lack of β-arrestin recruitment is likely due to the lack of serine and threonine residues in the A_1R cytoplasmic tail, which makes the A_1R intrinsically biased against β-arrestin signalling (*14, 26*).

The data from whole-cell patch-clamp recordings showed that BnOCPA did not influence neuronal membrane potential (Fig. 1G, H), while experiments in recombinant hA_1Rs showed that BnOCPA did not activate Goa (Fig. 2C, E). We thus predicted that A_1Rs in the hippocampus, where G_o is highly expressed (*27-29*), particularly at extra-synaptic sites (*30*),

should act via Goa to induce membrane hyperpolarisation. To test this we injected a series of previously validated interfering peptides (*31*) against Goa and Gob into CA1 pyramidal cells during whole-cell voltage clamp recordings. Introduction of the Goa interfering peptide caused a significant attenuation of the adenosine-induced outward current (Fig. 2G, H), whereas neither the scrambled peptide nor the Gob peptide had any effect on current amplitude (Fig. 2G, H). Thus, membrane potential hyperpolarisation occurs mainly through A_1R activation of Goa. The data from recombinant receptors demonstrating the inability of BnOCPA to activate Goa (Fig. 2C, E) thus explains why BnOCPA did not cause membrane hyperpolarisation, and indeed prevented or reversed the hyperpolarisation induced by CPA or adenosine, respectively (Fig. 1G, H; fig. S2A, C).

The signalling bias displayed by BnOCPA is reflected in non-canonical binding modes and a selective interaction with Gα subunits

To understand better the unusual signalling properties of BnOCPA and the highly specific Gα coupling, we carried out dynamic docking simulations to study the basic orthosteric binding mode of BnOCPA in an explicit, fully flexible environment using the active cryo-EM structure of the A_1R (PDB code 6D9H; Movie S1). We compared BnOCPA to the unbiased agonists adenosine and HOCPA, and an antagonist (PSB36) of the A_1R (Fig. 3A-C). BnOCPA engaged the receptor with the same fingerprint as adenosine (*32*) (Fig. 3A) and HOCPA, (Fig. 3B, Movie S2). Further explorations of the BnOCPA docked state using metadynamics revealed interchangeable variations on this fingerprint (namely modes A, B, and C; Fig. 3D - F; fig. S7) that could be distinguished by the orientation of the BnOCPA-unique benzyl (Bn) group. Having established the possible BnOCPA binding modes, we examined the respective contribution of the orthosteric agonists, the G protein α subunit α5 (C-terminal) helix (GαCT), and the Gα protein subunit (*33, 34*) to the empirically-observed G protein selectivity displayed by BnOCPA (Table 1, Fig. 2A-D, fig S3, S5).

Simulations in the absence of G protein. Firstly, following Dror et al., (*35*) we compared the dynamics of the BnOCPA-bound A_1R with the corresponding dynamics of the receptor (*36,*

37) bound to either HOCPA (Fig. 3B), the A_1R antagonist PSB36 (Fig 3C), or the apo receptor, our hypothesis being that there may be ligand-dependent differences in the way that the intracellular region of the receptor responds in the absence of the G protein. In these simulations the G protein was omitted so that inactivation was possible and so that the results were not G protein-dependent. The BnOCPA binding modes A-C were interchangeable during MD simulations (Methods Table 1) but were associated with distinctly different dynamics, as monitored by changes in a structural hallmark of GPCR activation, the $N^{7.49}PXXY^{7.53}$ motif (*38*) (fig. S8). Given the high flexibility shown by the BnOCPA benzyl group during the simulations and its lipophilic character, we hypothesized and simulated a further binding (namely Mode D) not explored during MD. This conformation involves a hydrophobic pocket underneath ECL3 (Fig 3G) which is responsible for the A_1/A_{2A} selectivity (*32*). Superimposition of the four BnOCPA binding modes (A-D) reveals the highly motile nature of the benzyl group of BnOCPA (Fig. 3H) under the simulated conditions.

Quantification of the $N^{7.49}PXXY^{7.53}$ dynamics revealed that HOCPA, BnOCPA mode A, BnOCPA mode C and the apo receptor show a similar distribution of the RMSD of the conserved $N^{7.49}PXXY^{7.53}$ motif (Fig. 3I; fig. S8). In contrast, the non-canonical BnOCPA binding modes B and D were responsible for a partial transition of the $N^{7.49}PXXY^{7.53}$ backbone from the active conformation to the inactive conformation (fig. S8) in a manner analogous with the antagonist PSB36 (Fig. 3J). Overall, the simulations revealed mode D as the most stable BnOCPA pose (6.8 μs out 9 μs simulated starting from this configuration – Methods Table 1), while mode B accounted for 3.6 μs out of 21 μs.

Dynamic Docking of GαCT. To simulate the agonist-driven interaction between the A_1R and the G protein, the α5 (C-terminal) helix (GαCT) of the G protein (Gi2, Goa, Gob) was dynamically docked to the HOCPA and BnOCPA-bound active A_1R structure (again lacking G protein; Movie S3). This allowed us to evaluate the effect of different GαCT on the formation of the complex with A_1R to test the hypothesis that, of Goa, Gob and Gi2, only the GαCT of

Gob would fully engage with the BnOCPA-bound active A_1R, in line with the empirical observations of G protein selectivity summarized in Table 1. Fig. 4A shows that the GαCT of Gob docked to the A_1R via a metastable state (MS1) relative to the canonical state (CS1; Movie S3), regardless of whether HOCPA or BnOCPA was bound. Fig. 4B,C show that the CS1 geometry corresponds to the canonical arrangement as found in the cryo-EM A_1R:G protein complex, whereas state MS1 resembles the recently reported non-canonical state observed in the neurotensin receptor, believed to be an intermediate on the way to the canonical state (*39*). In contrast, Fig. 4D-F show that the GαCT of Goa and Gi2 docks to the A_1R to form metastable states MS2 and MS3. MS2 is similar to the β_2-adrenergic receptor:GsCT fusion complex (*40*), proposed to be an intermediate on the activation pathway and a structure relevant to G protein specificity. In this case however, it appears to be on an unproductive pathway.

MD simulations on the full G protein. To test the hypothesis that the non-functional BnOCPA:A_1R:Goa complex showed anomalous dynamics, we increased the complexity of the simulations by considering the Gα subunit of the Goa and Gob protein bound to the A_1R:BnOCPA (mode B or D) complex or the Gob protein bound to A_1R:HOCPA (a functional system). The most visible differences between Goa (Movie 4) and Gob (Movie 5) comprised the formation of transient hydrogen bonds between the α4-β6 and α3-β5 loops of Goa and helix 8 (H8) of the receptor (table S2). Similar contacts are present in the non-canonical state of the neurotensin receptor:G protein complex (*39*). Overall, Goa interacted more with TM3 and ICL2 residues (Fig. 4G, H), while TM5 and TM6, along with ICL1, were more engaged by Gob (Fig 4G, H). Interestingly, R291$^{7.56}$ and I292$^{8.47}$, which are located under the N$^{7.49}$PXXY$^{7.53}$ motif, showed a different propensity to interact with Goa or Gob. In this scenario, it is plausible that a particular A_1R conformation stabilized by BnOCPA (as suggested by the simulations in the absence of G protein, Fig 3I-J) may favor different intermediate states during the activation process of Goa and Gob.

In vivo physiological validation of BnOCPA-mediated signalling bias

Given BnOCPA's clear differential effects in a native physiological system (Fig. 1), strong Gα bias (Fig. 2), unique binding characteristics (Fig. 3) and selective Gα interaction (Fig. 4) we hypothesised that these properties might circumvent a key obstacle to the development of A_1R agonists for therapeutic use - their powerful effects in the cardiovascular system (CVS) where their activation markedly reduces both heart rate and blood pressure (*41*). As these CVS effects are likely through Goa, which is expressed at high levels in the heart (*42, 43*) and plays an important role in regulating cardiac function (*27*), the lack of effect of BnOCPA on Goa (Fig. 2C, E; fig S5) predicted that BnOCPA would have minimal effects on the CVS.

In initial experiments we screened BnOCPA for its effects on heart rate using an isolated frog heart preparation. In contrast to adenosine and CPA, BnOCPA had no effect on heart rate, but markedly reduced the bradycardia evoked by adenosine (fig. S9A). Thus, BnOCPA appears not to activate A_1Rs in the heart, but instead behaves like an antagonist in preventing the actions of the endogenous agonist. These observations have parallels in BnOCPA inhibiting or reversing the postsynaptic hyperpolarisation induced by typical A_1R agonists (Fig. 1G, H; fig. S2), and in preventing the inhibition of cAMP accumulation by adenosine (Fig. 2F). Such antagonist-like behaviour may be explained by BnOCPA causing unique A_1R conformations unlike those of conventional agonists (Fig. 3I, J), and driving non-canonical interactions with Goa (Fig. 4).

To investigate the effects of BnOCPA in an intact mammalian system, we measured the influence of BnOCPA on heart rate and blood pressure in urethane-anaesthetised, spontaneously breathing adult rats. As expected, both resting heart rate and arterial blood pressure were significantly reduced by adenosine and CPA (Fig. 5A to D). In complete contrast, BnOCPA had no effect on either heart rate (Fig. 5A, C) or blood pressure (Fig. 5B, D). Moreover, when co-applied with adenosine, BnOCPA abolished the bradycardia induced by adenosine, indicating its ability to bind to the A_1R at the dose applied (Fig. 5A, C; fig. S9B). The rapid early effects of adenosine on blood pressure, likely due to bradycardia, were blocked

by BnOCPA, but the slower component was unaffected by BnOCPA (Fig. 5B, D; fig. S9B). Volumes of saline equivalent to the drug injections had no effect on either heart rate or blood pressure and there was no waning in the effects of adenosine responses with repeated doses (fig. S9C, D). Thus, BnOCPA does not appear to act as an agonist at CVS A_1Rs, but instead antagonises the bradycardic effects of A_1R activation on the heart. Since adverse effects on respiration (dyspnea) limit the use of systemic A_1R agonists (*5*), we additionally examined the effects of BnOCPA on respiration. In urethane-anaesthetised, spontaneously breathing adult rats, intravenous injection of the selective A_1R agonist CPA caused significant respiratory depression (Fig. 6A to D). In stark contrast, BnOCPA had no appreciable effect on respiration (Fig. 6A to D).

BnOCPA is a potent analgesic

These observations, of a lack of effect of BnOCPA on the CVS and respiration, prompted an investigation into a potential application of A_1R agonists that had previously been severely curtailed by adverse cardiorespiratory events (*5*): A_1R agonists as analgesics. To test BnOCPA's potential as an analgesic, we used a rat model of chronic neuropathic pain (spinal nerve ligation) a feature of which is mechanical allodynia whereby the affected limb is rendered sensitive to previously innocuous tactile stimuli. Both intravenous (Fig. 6E) and intrathecal (Fig. 6F) BnOCPA potently reversed mechanical allodynia in a dose-dependent manner but had no depressant effects on motor function that might be mistaken for true analgesia (fig. S10). Thus, BnOCPA exhibits powerful analgesic properties at doses devoid of cardiorespiratory effects and at several orders of magnitude lower than the non-opioid analgesics pregabalin and gabapentin (*44*).

Discussion

Biased agonists at GPCRs offer great potential for the selective activation of desirable intracellular signalling pathways, while avoiding, or indeed blocking those pathways that lead to adverse or unwanted effects (*2*). While this, and the potential to exploit previously unattractive drug targets such as the A_1R, have been appreciated, translation of *in vitro* observations, particularly of Gα bias, to native receptors *in vivo* has been problematic (*2, 15*). Here we have shown that translation of *in vitro* Gα signalling bias to an intact physiological system is possible. Moreover, this has occurred in the context of the A_1R, an attractive, but notoriously intractable drug target by virtue of the profound cardiorespiratory consequences of its activation.

Having identified BnOCPA as a biased agonist for the A_1R *in vitro*, we have discovered that native A_1Rs can be induced to selectively activate specific Gα subunits, and that BnOCPA has unique properties in doing so when compared with other A_1R agonists. This effect is evident at both recombinant and native A_1Rs in both the CNS and CVS. Moreover, these properties of BnOCPA were observed at A_1Rs expressed by three different species: amphibian, rat, and human. While BnOCPA induced A_1R coupling to Gα subunits activated by prototypical A_1R agonists such as adenosine and CPA, it did not activate Goa. This likely reflects BnOCPA's non-canonical binding profile at the A_1R, which had profound implications for the interaction with the GαCT in terms of different binding pathways and intermediate states, and in the different intra- and intermolecular hydrogen bond patterns and contacts observed in the simulations of the A_1R in complex with either Goa or Gob. These differences are likely to underlie the ability of the BnOCPA-bound A_1R to selectively trigger Gob activation.

The unique and unprecedented bias displayed by BnOPCA has physiological importance since it is able to inhibit excitatory synaptic transmission without causing neuronal membrane hyperpolarisation, bradycardia, hypotension or dyspnea. BnOCPA thus overcomes cardiovascular and respiratory obstacles to the development of adenosine-based therapeutics

that have plagued the field since their first description nine decades ago (*46*). As a first, but significant, step towards this, we demonstrate that BnOCPA has powerful analgesic properties in an *in vivo* model of chronic neuropathic pain, a condition for which the current treatments are either severely lacking in efficacy or, in the case of opioids, come with unacceptable respiratory depression, tolerance, dependence and abuse potential. We have thus shown for the first time that native A_1Rs can be induced to signal via distinct Gα subunits to mediate differential physiological effects, and have identified a novel molecule capable of doing so. We have also explored molecular mechanisms by which this could occur, and demonstrated pain as one potential and wide-reaching therapeutic application. Such discoveries are of importance in both understanding GPCR-mediated signalling, and in the generation of both new research tools and therapeutics based on the untapped potential of biased agonists.

Acknowledgements: We gratefully acknowledge the support of the University of Warwick (URSS Awards to SH and JO; Warwick Ventures Proof of Concept Fund awards to MJW & BGF), the Leverhulme Trust (RPG-2017-255, CAR and GL to fund KB and GD), the BBSRC (BB/M00015X/2, GL and BB/M01116X/1, PhD studentship to EH), the MRC (MR/J003964/1; IW) and The Swiss National Science Foundation (PP00P2_146321, MLo). RH is supported by an MRC Discovery Award (MC_PC_15070). CAR is a Royal Society Industry Fellow. We would like to thank Stephen Hill, Stephen Briddon and Mark Soave (University of Nottingham) for gifting the A_3R-Nluc construct, and Kathleen Caron and Duncan Mackie (University of North Carolina) for the β-arrestin2-YFP construct. We are grateful to Professor Kevin Moffat and the Biochemistry students of the School of Life Sciences at the University of Warwick for access to their frog heart preparations, and to Professor Nick Dale, Dr Mark Wigglesworth and Dr Jens Kleinjung for discussions and comments on draft manuscripts. *In vivo* studies on neuropathic pain were funded and undertaken by NeuroSolutions Ltd.

Author Contributions: Experiments were designed by MJW, RH, CAR, GL, FYZ, DS, BGF, and were performed by MJW, EH, RH, KB, IW, HFW, WI, ED, CH, JO, SH. Compounds were synthesised by MLe, BP, MLo. Molecular docking simulations were carried out by GD and CAR. Work was originally conceived by MJW and BGF. The manuscript was written by MJW and BGF with comments on drafts from EH, RH, MLo, GL, IW, KB, GD, CAR, IM and DS.

Conflict of Interest: The University of Warwick has filed a patent application for uses of BnOCPA. FYZ, HFW and DS are employees and/or hold shares in NeuroSolutions.

Data Availability: The data and materials that support the findings of this study are available from the corresponding author upon reasonable request.

Supplementary Materials:

Materials and Methods

Supplemental Figures S1 – S10

Supplemental Tables S1 – S2

Supplemental Movies S1 – S5

References

1. A. S. Hauser, M. M. Attwood, M. Rask-Andersen, H. B. Schiöth, D. E. Gloriam, Trends in GPCR drug discovery: new agents, targets and indications. *Nature Reviews Drug Discovery* **16**, 829 (2017).
2. T. Kenakin, Is the Quest for Signaling Bias Worth the Effort? *Mol Pharmacol* **93**, 266-269 (2018).
3. K. A. Jacobson, C. E. Muller, Medicinal chemistry of adenosine, P2Y and P2X receptors. *Neuropharmacology* **104**, 31-49 (2016).
4. P. A. Borea, S. Gessi, S. Merighi, F. Vincenzi, K. Varani, Pharmacology of Adenosine Receptors: The State of the Art. *Physiol Rev* **98**, 1591-1625 (2018).
5. J. Sawynok, Adenosine receptor targets for pain. *Neuroscience* **338**, 1-18 (2016).
6. J. P. Headrick, K. J. Ashton, R. B. Rose'meyer, J. N. Peart, Cardiovascular adenosine receptors: expression, actions and interactions. *Pharmacol Ther* **140**, 92-111 (2013).
7. T. V. Dunwiddie, S. A. Masino, The role and regulation of adenosine in the central nervous system. *Annu Rev Neurosci* **24**, 31-55 (2001).
8. E. A. Vecchio *et al.*, New paradigms in adenosine receptor pharmacology: allostery, oligomerization and biased agonism. *Br J Pharmacol* **175**, 4036-4046 (2018).
9. K. Varani, F. Vincenzi, S. Merighi, S. Gessi, P. A. Borea, Biochemical and Pharmacological Role of A1 Adenosine Receptors and Their Modulation as Novel Therapeutic Strategy. *Adv Exp Med Biol* **1051**, 193-232 (2017).
10. J. A. Baltos *et al.*, Quantification of adenosine A(1) receptor biased agonism: Implications for drug discovery. *Biochem Pharmacol* **99**, 101-112 (2016).
11. L. Weltha, J. Reemmer, D. Boison, The role of adenosine in epilepsy. *Brain Res Bull*, (2018).
12. T. Kenakin, Biased Receptor Signaling in Drug Discovery. *Pharmacol Rev* **71**, 267-315 (2019).
13. D. Wootten, A. Christopoulos, M. Marti-Solano, M. M. Babu, P. M. Sexton, Mechanisms of signalling and biased agonism in G protein-coupled receptors. *Nat Rev Mol Cell Biol* **19**, 638-653 (2018).
14. J. D. Violin, R. J. Lefkowitz, Beta-arrestin-biased ligands at seven-transmembrane receptors. *Trends Pharmacol Sci* **28**, 416-422 (2007).

15. M. C. Michel, S. J. Charlton, Biased Agonism in Drug Discovery-Is It Too Soon to Choose a Path? *Mol Pharmacol* **93**, 259-265 (2018).

16. Y. Cordeaux, A. P. Ijzerman, S. J. Hill, Coupling of the human A1 adenosine receptor to different heterotrimeric G proteins: evidence for agonist-specific G protein activation. *Br J Pharmacol* **143**, 705-714 (2004).

17. G. D. Stewart *et al.*, Determination of adenosine A1 receptor agonist and antagonist pharmacology using Saccharomyces cerevisiae: implications for ligand screening and functional selectivity. *J Pharmacol Exp Ther* **331**, 277-286 (2009).

18. C. Valant *et al.*, Separation of on-target efficacy from adverse effects through rational design of a bitopic adenosine receptor agonist. *Proc Natl Acad Sci U S A* **111**, 4614-4619 (2014).

19. L. Aurelio *et al.*, A Structure-Activity Relationship Study of Bitopic N(6)-Substituted Adenosine Derivatives as Biased Adenosine A1 Receptor Agonists. *J Med Chem* **61**, 2087-2103 (2018).

20. A. Knight *et al.*, Discovery of novel adenosine receptor agonists that exhibit subtype selectivity. *J Med Chem* **59**, 947-964 (2016).

21. F. Ciruela *et al.*, Ligand-induced phosphorylation, clustering, and desensitization of A1 adenosine receptors. *Mol Pharmacol* **52**, 788-797 (1997).

22. S. Gines *et al.*, Involvement of caveolin in ligand-induced recruitment and internalization of A(1) adenosine receptor and adenosine deaminase in an epithelial cell line. *Mol Pharmacol* **59**, 1314-1323 (2001).

23. M. Escriche *et al.*, Ligand-induced caveolae-mediated internalization of A1 adenosine receptors: morphological evidence of endosomal sorting and receptor recycling. *Exp Cell Res* **285**, 72-90 (2003).

24. L. Iacovelli, R. Franchetti, D. Grisolia, A. De Blasi, Selective regulation of G protein-coupled receptor-mediated signaling by G protein-coupled receptor kinase 2 in FRTL-5 cells: analysis of thyrotropin, alpha(1B)-adrenergic, and A(1) adenosine receptor-mediated responses. *Mol Pharmacol* **56**, 316-324 (1999).

25. G. Ferguson, K. R. Watterson, T. M. Palmer, Subtype-specific regulation of receptor internalization and recycling by the carboxyl-terminal domains of the human A1 and rat A3 adenosine receptors: consequences for agonist-stimulated translocation of arrestin3. *Biochemistry* **41**, 14748-14761 (2002).

26. W. Yin *et al.*, A complex structure of arrestin-2 bound to a G protein-coupled receptor. *Cell Res* **29**, 971-983 (2019).

27. M. Jiang, N. S. Bajpayee, Molecular mechanisms of Go signaling. *Neurosignals* **17**, 23-41 (2009).

28. P. F. Worley, J. M. Baraban, C. Van Dop, E. J. Neer, S. H. Snyder, Go, a guanine nucleotide-binding protein: immunohistochemical localization in rat brain resembles distribution of second messenger systems. *Proc Natl Acad Sci U S A* **83**, 4561-4565 (1986).

29. T. Terashima, T. Katada, M. Oinuma, Y. Inoue, M. Ui, Immunohistochemical analysis of the localization of guanine nucleotide-binding protein in the mouse brain. *Brain Res* **442**, 305-311 (1988).

30. J. Gabrion *et al.*, Ultrastructural localization of the GTP-binding protein Go in neurons. *Cell Signal* **1**, 107-123 (1989).

31. A. Gilchrist, A. Li, H. E. Hamm, G alpha COOH-terminal minigene vectors dissect heterotrimeric G protein signaling. *Sci STKE* **2002**, pl1 (2002).

32. R. K. Y. Cheng *et al.*, Structures of Human A1 and A2A Adenosine Receptors with Xanthines Reveal Determinants of Selectivity. *Structure* **25**, 1275-1285.e1274 (2017).

33. T. Flock *et al.*, Selectivity determinants of GPCR-G-protein binding. *Nature* **545**, 317-322 (2017).

34. N. Okashah *et al.*, Variable G protein determinants of GPCR coupling selectivity. *Proc Natl Acad Sci U S A* **116**, 12054-12059 (2019).

35. R. O. Dror *et al.*, Activation mechanism of the β2-adrenergic receptor. *Proc Natl Acad Sci USA* **108**, 18684-18689 (2011).

36. C. J. Draper-Joyce *et al.*, Structure of the adenosine-bound human adenosine A1 receptor-Gi complex. *Nature* **558**, 559-563 (2018).

37. A. Glukhova *et al.*, Structure of the Adenosine A1 Receptor Reveals the Basis for Subtype Selectivity. *Cell* **168**, 867-877 e813 (2017).

38. D. M. Rosenbaum, S. G. Rasmussen, B. K. Kobilka, The structure and function of G-protein-coupled receptors. *Nature* **459**, 356-363 (2009).

39. H. E. Kato *et al.*, Conformational transitions of a neurotensin receptor 1-Gi1 complex. *Nature* **572**, 80-85 (2019).

40. X. Liu *et al.*, Structural Insights into the Process of GPCR-G Protein Complex Formation. *Cell* **177**, 1243-1251 e1212 (2019).

41. M. Koeppen, T. Eckle, H. K. Eltzschig, Selective deletion of the A1 adenosine receptor abolishes heart-rate slowing effects of intravascular adenosine in vivo. *PLoS One* **4**, e6784 (2009).

42. T. Asano *et al.*, The G-protein G(o) in mammalian cardiac muscle: localization and coupling to A1 adenosine receptors. *J Biochem* **117**, 183-189 (1995).

43. W. P. Wolf, K. Spicher, H. Haase, W. Schulze, Immunocytochemical localization of the G-protein sub-unit, G(o) alpha, in rat heart. Implications for a role of G(o) alpha in secretion of cardiac hormones. *J Mol Cell Cardiol* **30**, 1149-1162 (1998).

44. M. Chincholkar, Analgesic mechanisms of gabapentinoids and effects in experimental pain models: a narrative review. *Br J Anaesth* **120**, 1315-1334 (2018).

45. M. Z. Imam, A. Kuo, S. Ghassabian, M. T. Smith, Progress in understanding mechanisms of opioid-induced gastrointestinal adverse effects and respiratory depression. *Neuropharmacology* **131**, 238-255 (2018).

46. A. N. Drury, A. Szent-Gyorgyi, The physiological activity of adenine compounds with especial reference to their action upon the mammalian heart. *J Physiol* **68**, 213-237 (1929).

Table 1

Agonist	IC_{50} (nM)	Gα subunits					
		Gi1	Gi2	Gi3	Goa	Gob	Gz
Adenosine	3.5						
CPA	0.5						
NECA	0.2						
BnOCPA	0.7						
HOCPA	0.8						

Summary of Gα activation by selective A_1R agonists; Green boxes indicate activation; Grey boxes indicated no activation. Indicative IC_{50} values for inhibition of cAMP production in CHO-K1 cells derived from the mean pIC_{50} values reported in table S1. Data taken from: Adenosine, CPA, BnOCPA Fig.2, fig. S3; NECA, fig. S3; HOCPA, fig. S4.

Fig. 1. BnOCPA discriminates between pre- and postsynaptic A_1Rs in the CNS

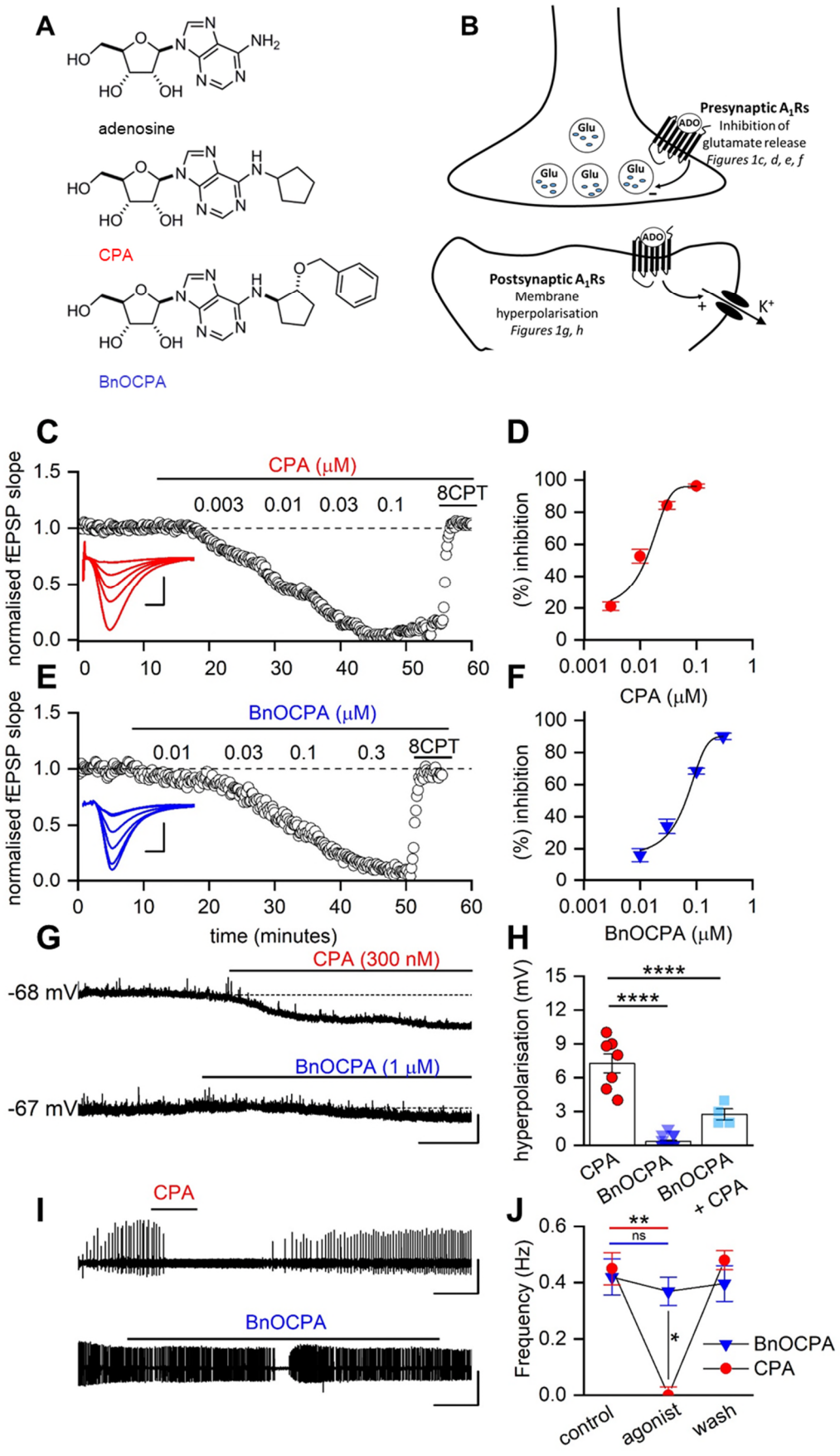

Fig. 1. BnOCPA discriminates between pre- and postsynaptic A_1Rs in the CNS

(A), Chemical structures of adenosine, CPA and its derivative, BnOCPA (*20*). **(B)**, Diagram illustrating pre- and postsynaptic A_1Rs at hippocampal synapses, their physiological effects upon activation, and the panels in Figure 1 where these effects can be seen. **(C)** Increasing concentrations of the A_1R agonist CPA reduced the field excitatory postsynaptic potential (fEPSP), an effect reversed by the A_1R antagonist 8CPT (2 μM). The graph plots the normalised negative slope of the fEPSP, an index of the strength of synaptic transmission, over time. Inset, superimposed fEPSP averages in control (largest fEPSP) and becoming smaller in increasing concentrations of CPA. Scale bars measure 0.2 mV and 5 ms. **(D)**, Concentration-response curve for the inhibition of synaptic transmission by CPA (IC_{50} = 11.8 ± 2.7 nM; *n* = 11 slices). **(E),** Increasing concentrations of BnOCPA reduced the fEPSP, an effect reversed by 8CPT (2 μM). Inset, superimposed fEPSP averages in control and in increasing concentrations of BnOCPA. Scale bars measure 0.1 mV and 2 ms. **(F)**, Concentration-response curve for the inhibition of synaptic transmission by BnOCPA (IC_{50} = 65 ± 0.3 nM; *n* = 11 slices). **(G)**, CPA (300 nM) hyperpolarised the membrane potential while BnOCPA (1 μM) had little effect. Scale bars measure 4 mV and 30 s. **(H)**, Summary data for membrane potential changes. The mean hyperpolarisation produced by CPA (300 nM; 7.26 ± 0.86 mV, *n* = 7 cells) was significantly different (one-way ANOVA; F(2,23) = 70.46; P = 1.55 x 10^{-10}) from that produced by BnOCPA (300 nM - 1 μM; 0.33 ± 0.14 mV, *n* = 10 and 5 cells, respectively; P = 8.26 x 10^{-11}) and for CPA (300 nM) applied in the presence of BnOCPA (300 nM; 2.75 ± 0.48 mV, n = 4 cells, P = 2.89 x 10^{-5}; fig. 2a for an example trace). **(I)**, In an *in vitro* model of seizure activity, represented as frequent spontaneous spiking from baseline, CPA (300 nM) reversibly blocked activity while BnOCPA (300 nM) had little effect. Scale bars measure 0.5 mV and 200 s. **(J)**, Summary data for seizure activity expressed in terms of the frequency of spontaneous spiking before, during and after CPA or BnOCPA. CPA abolished seizure activity (*n* = 4) whereas BnOCPA did not significantly reduce seizure frequency (*n* = 6). Data represented as mean ± SEM; Two-way RM ANOVA (BnOCPA vs CPA slices): F(1,

3) = 186.11, P = 8.52 x10^{-4} with the following Bonferroni post hoc comparisons: BnOCPA vs Control; P = 1; CPA vs control; P = 0.010; BnOCPA vs CPA; P = 0.027. Averaged data is presented as mean ± SEM. ns, not significant; ∗, P < 0.05; ∗∗, P < 0.02; ∗∗∗∗, P < 0.0001.

Fig. 2. Differential G protein activation profile of BnOCPA compared to prototypical A_1R agonists.

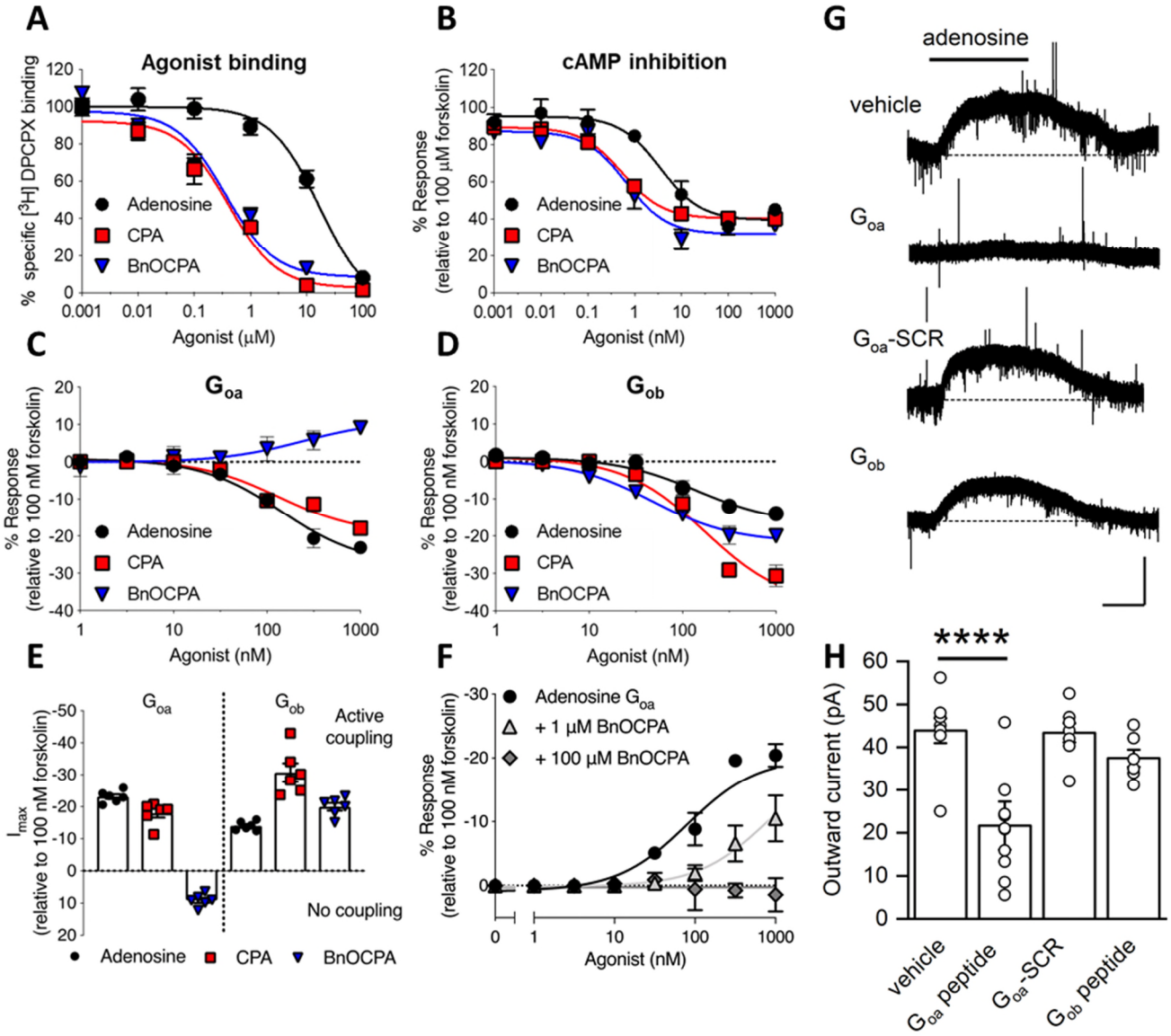

Fig. 2. Differential G protein activation profile of BnOCPA compared to prototypical A_1R agonists.

(A), The binding of adenosine, CPA and BnOCPA to the human (h) A_1R was measured via their ability to displace [^{3}H]DPCPX, a selective antagonist for the A_1R, from membranes prepared from CHO-K1-hA_1R cells. The data indicate that CPA and BnOCPA bind with equal affinity to the A_1R, while adenosine has a reduced affinity (*n* = 5 - 19 individual repeats). **(B),** cAMP levels were measured in CHO-K1-hA_1R cells following co-stimulation with 1 μM forskolin and each compound (1 pM - 1 μM) for 30 minutes. This identified that all are full agonists. Adenosine displays a 10-fold reduced potency compared to CPA and BnOCPA (*n* = 4 individual repeats). **(C),** cAMP accumulation was measured in PTX-pre-treated (200 ng/ml) CHO-K1-hA_1R cells expressing PTX-insensitive Goa following co-stimulation with 1 μM forskolin and each compound (1 pM - 1 μM) for 30 minutes (*n* = 6 individual repeats). The data demonstrates that BnOCPA does not activate Goa. **(D)**, as for **(C)**, but cells were transfected with PTX-insensitive Gob. Adenosine, CPA and BnOCPA all inhibit cAMP accumulation through coupling to Gob (*n* = 6 individual repeats). **(E)**, Summary of maximal A_1R-stimulated inhibition of cAMP by adenosine, CPA and BnOCPA in CHO-K1-hA_1R cells expressing either Goa (left) or Gob (right) obtained from data in panels **(C)** and **(D)**. **(F)**, Adenosine's ability to inhibit cAMP accumulation via its activation of Goa was inhibited by BnOCPA in a concentration-dependent manner and with a Kd of 113 nM (*n* = 4 individual repeats). **(G)**, Example current traces produced by adenosine (10 μM) in control conditions, in the presence of intracellular Goa peptide (100 μM), scrambled Goa peptide (SCR; 100 μM) and Gob peptide (100 μM). Scale bars measure 50 pA and 100 s. **(H)**, Summary data of outward current experiments. The mean amplitude of the outward current induced by adenosine (43.9 ± 3.1 pA, *n* = 8 cells) was significantly reduced (one-way ANOVA; $F(3,27) = 13.31$, $P = 1.60 \times 10^{-5}$) to 20.9 ± 3.6 pA (*n* = 10 cells, $P = 5.35 \times 10^{-5}$) in 100 μM Goa peptide. Neither the scrambled peptide (43.4 ± 2.4 pA, *n* = 7 cells, P = 1) nor the Gob peptide (37. 4 ± 2.2 pA, *n* = 6 cells, P =

1) significantly reduced the amplitude of the adenosine-induced outward current. Averaged data is presented as mean ± SEM. ****, $P < 0.0001$

Fig. 3. Molecular dynamics simulations reveal that BnOCPA binding modes can drive both agonist- and antagonist-like intracellular conformations of the A_1R.

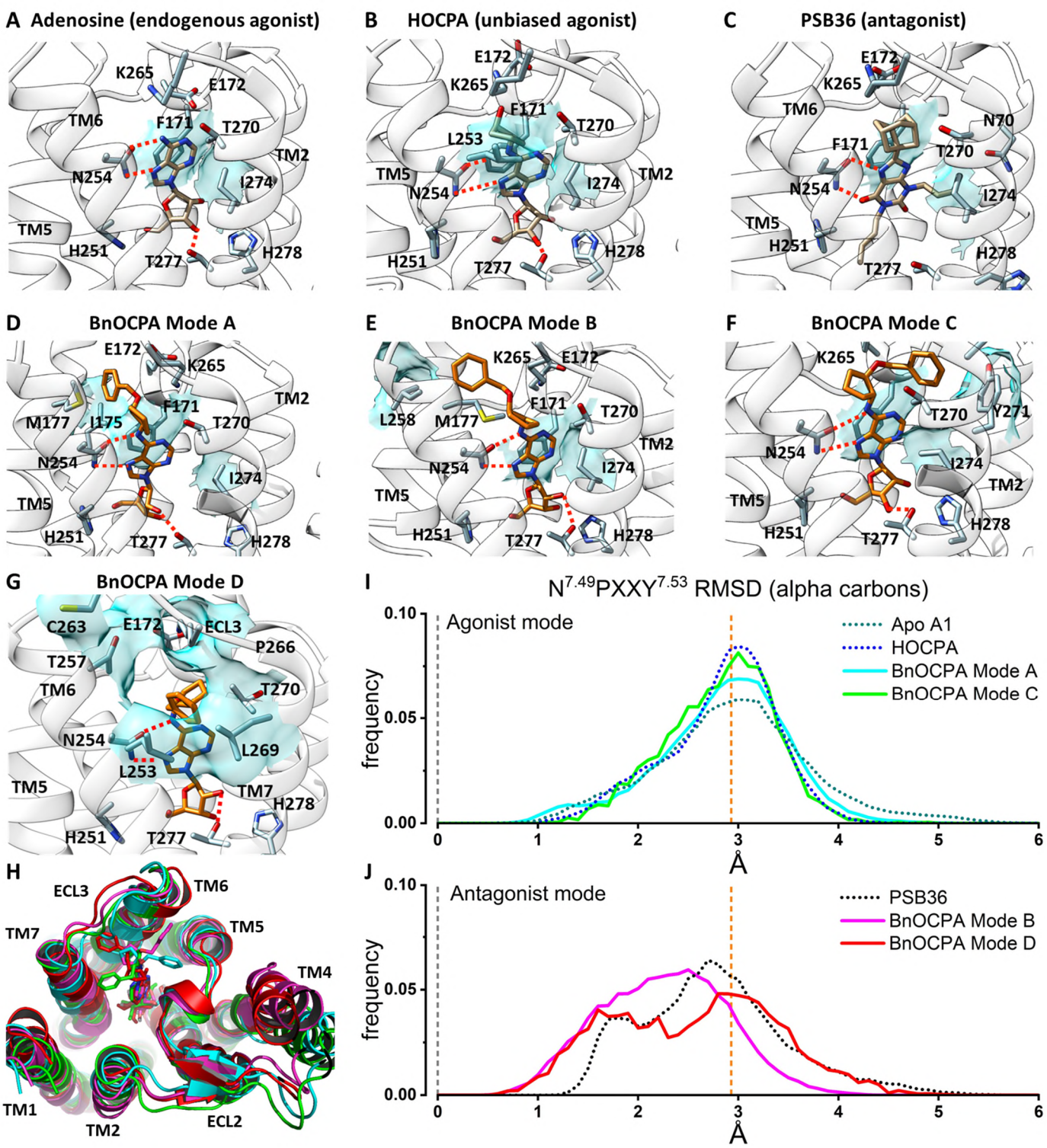

Fig. 3. Molecular dynamics simulations reveal that BnOCPA binding modes can drive both agonist- and antagonist-like intracellular conformations of the A_1R.

(A), Adenosine binding pose: N254$^{6.55}$ (Ballesteros-Weinstein superscript enumeration) is engaged in key hydrogen bonds, while important hydrophobic contacts are shown as cyan transparent surfaces (F171^{ECL2} and I274$^{7.39}$). **(B)**, On the basis of structural similarities and the dynamic docking (Movie S2), HOCPA was predicted to bind with a geometry analogous to adenosine; the cyclopentyl group makes further hydrophobic contacts with L253$^{6.54}$, as shown by simulation. **(C)**, The xanthine scaffold of the antagonist PSB36 makes hydrogen bonds with N254$^{6.55}$ side chains and hydrophobic contacts with F171^{ECL2} and I274$^{7.39}$. **(D)**, BnOCPA agonist-like binding Mode A (Movie S1): the benzyl group orients towards the ECL2 and makes hydrophobic contacts with I175^{ECL2} (and M177$^{5.35}$) side chains. **(E)**, BnOCPA antagonist-like binding Mode B: the benzyl group orients towards the top of TM5/TM6 and makes hydrophobic contacts with L258$^{6.59}$ side chain. **(F)**, BnOCPA agonist-like binding Mode C: the benzyl group orients towards the top of TM7 and makes hydrophobic contacts with Y271$^{7.36}$ side chain. **(G)** Binding orientation of BnOCPA in antagonist Mode D: the benzyl group orients under ECL3 and occupies the hydrophobic pocket defined by L253$^{6.54}$, T257$^{6.58}$, T270$^{7.35}$, and L269$^{7.34}$. Key hydrogen bonds with N254$^{6.55}$ and T277$^{7.42}$ are shown as dotted lines; main hydrophobic contacts are highlighted as cyan transparent surfaces. **(H)** Extracellular view of the A_1R showing the four BnOCPA binding modes A (cyan), B (magenta), C (green), and D (red) as randomly extracted from the MD simulations. **(I, J)**, Root-mean-square deviation (RMSD) distributions considering the inactive N$^{7.49}$PXXY$^{7.53}$ motif on the distal part of TM7 as reference. **(I)**, HOCPA (blue broken line), BnOCPA Mode A (cyan curve), BnOCPA Mode C (green curve) and the apo receptor (dark green broken line) have a common distribution centring around the active confirmation of the A_1R (orange broken line; fig. S7), whereas **(J)**, PSB36 (black broken line), BnOCPA Mode B (magenta curve) and BnOCPA Mode D (red curve) RMSD values have the tendency to move closer to the inactive N$^{7.49}$PXXY$^{7.53}$ geometry (leftward shift of the curves towards broken grey line at x = 0)

Figure 4. Binding differences between the terminal helix 5 (GαCT) of cognate and non-cognate Gα subunits and Goa and Gob during dynamic docking to the biased BnOCPA-A_1R and unbiased HOCPA-A_1R complexes.

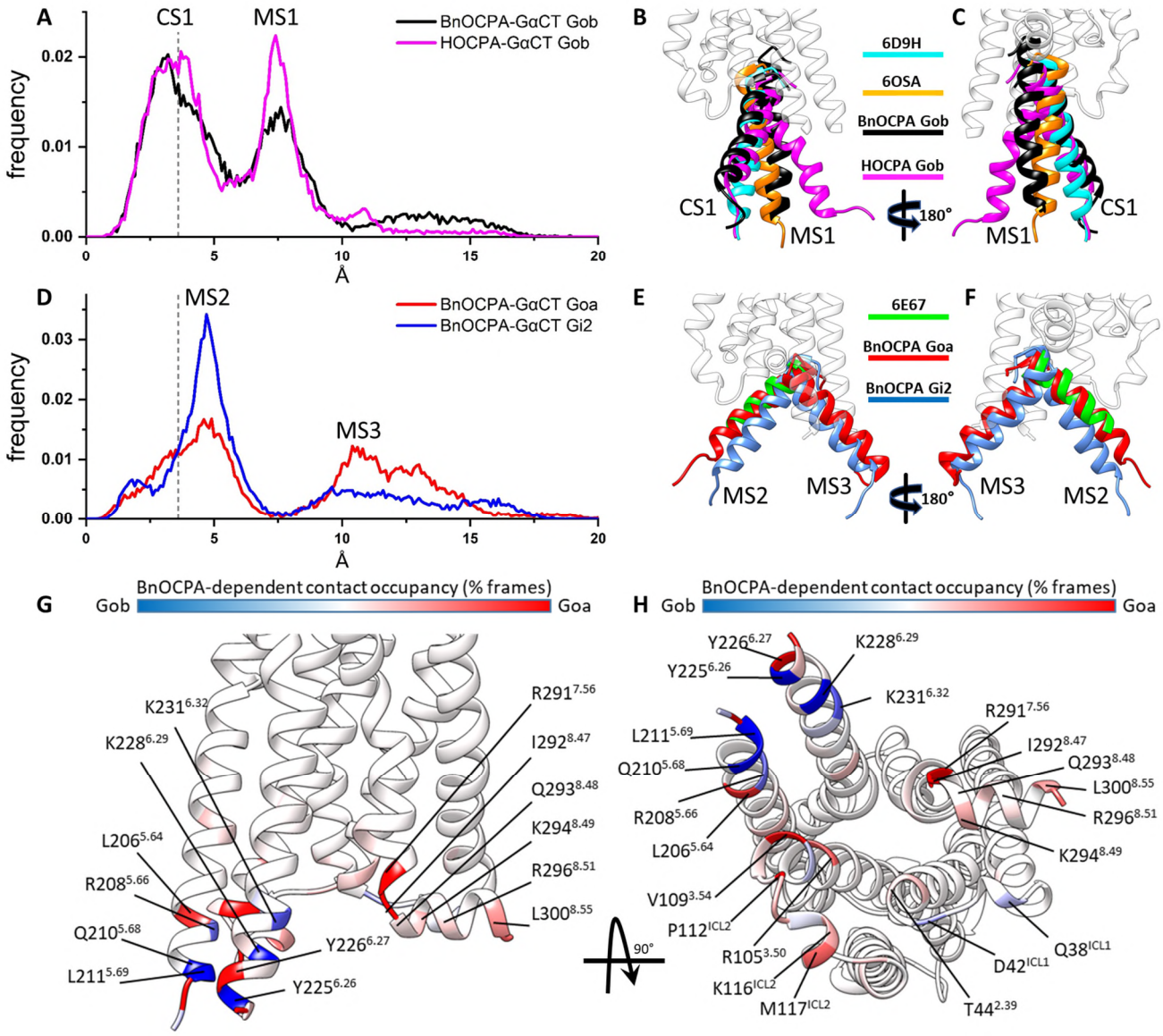

Figure 4. Binding differences between the terminal helix 5 (GαCT) of cognate and non-cognate Gα subunits and Goa and Gob during dynamic docking to the biased BnOCPA-A_1R and unbiased HOCPA-A_1R complexes.

(**A, B, C**) Dynamic docking of the Gob GαCT (last 27 residues) performed on the BnOCPA-A_1R (black) and the HOCPA-A_1R (magenta) complex, respectively. (**A**) Frequency distribution of the RMSD of the last 15 residues of GαCT (alpha carbon atoms) to the Gi2 GαCT conformation reported in the A_1R cryo-EM structure 6D9H (the 3.6Å resolution of which is indicated by the dashed grey line): the two most probable RMSD ranges, namely canonical state CS1 and metastable state MS1, can be observed. (**B, C**) Two side views of representative MD frames of the most populated α5 clusters from the states CS1 and MS1. The last 15 residues of Gob GαCT in the CS1 states of both BnOCPA (black) and HOCPA (magenta) resemble the experimental Gi2 bound state (PDB code 6D9H - cyan). The alternative highly populated MS1 state is characterized by a binding geometry similar to the non canonical Gi intermediate state reported in the neurotensin receptor structure 6OSA (orange). (**D, E, F**) Dynamic docking of the Goa (red) and Gi2 (blue) GαCT (last 27 residues) performed on the BnOCPA-A_1R complex. (**D**) Frequency distribution of the RMSD of the GαCT last 15 residues (alpha carbon atoms) to the Gi2 GαCT conformation reported in the A_1R cryo-EM structure 6D9H (the resolution of which, 3.6Å, is indicated by the dashed grey line): the two most probable RMSD ranges are labelled as MS2 and MS3. (**E, F**) Two side views of representative MD frames of the most populated GαCT clusters from the states MS2 and MS3; the Goa (red) and Gi2 (blue) last 15 residues in the state MS2 overlap well with the putative Gs intermediate state (PDB code 6E67 - green). In the alternative highly populated state MS3, the GαCT helix orients in unique conformations that differ from those previously described. **(G, H)** For each residue the interaction plotted on the backbone is the difference between the Goa and Gob occupancies in the presence of orthosteric BnOCPA (% of MD frames in which interaction occurred). BnOCPA/A_1R/Goa had the tendency to more interact with ICL2, TM3 TM7, and H8 (red), while BnOCPA/A_1R/Gob formed more contacts with TM5 and TM6 (blue).

Fig. 5. BnOCPA does not affect heart rate or blood pressure

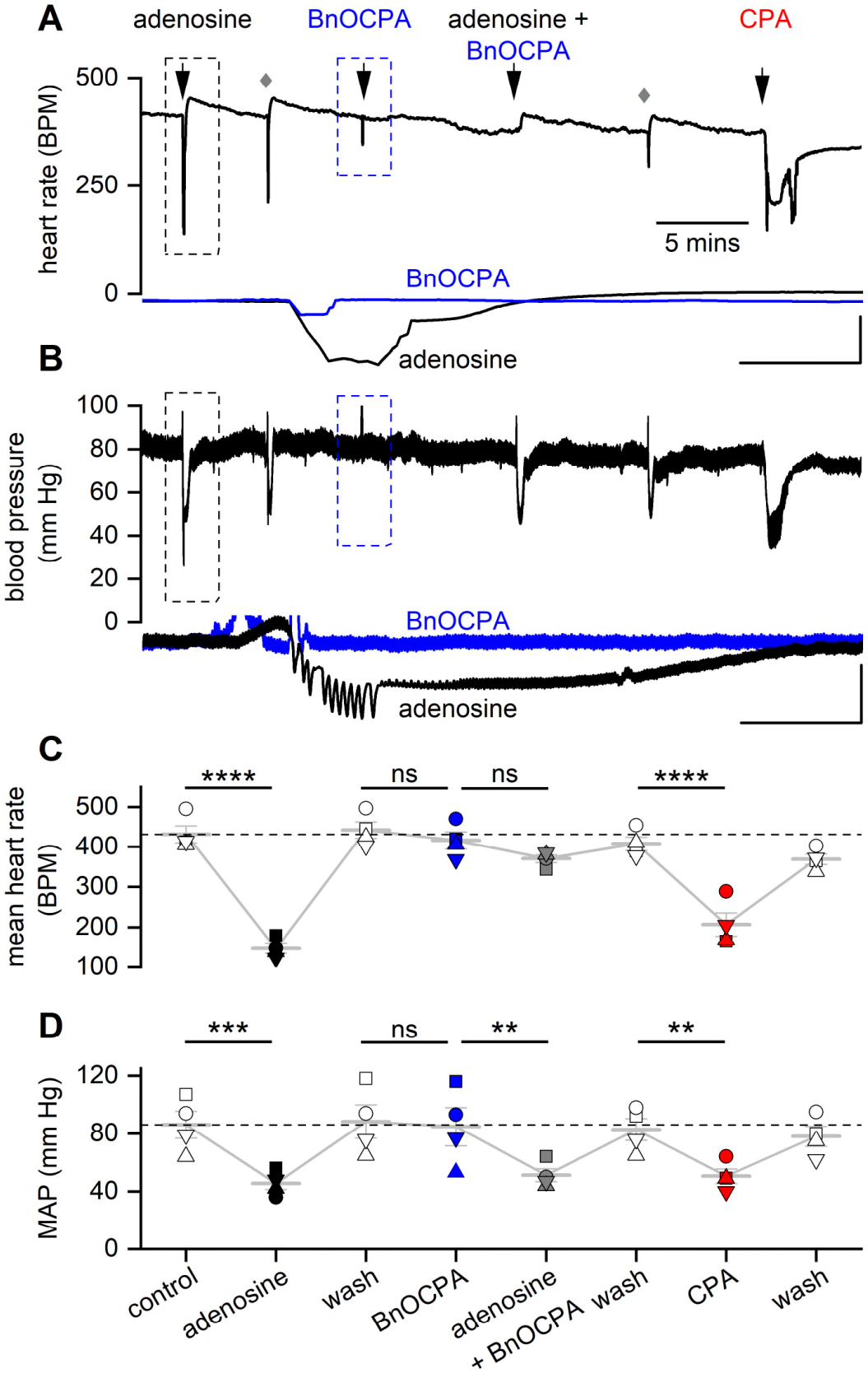

Fig. 5. BnOCPA does not affect heart rate or blood pressure

(A), Examples of heart rate (HR) and **(B),** blood pressure traces from a single urethane-anaesthetised, spontaneously breathing rat showing the effects of adenosine (1 $mg \cdot kg^{-1}$), BnOCPA (8.3 $\mu g \cdot kg^{-1}$) and CPA (6.3 $\mu g \cdot kg^{-1}$). Adenosine, BnOCPA and CPA were given as a 350 $\mu L \cdot kg^{-1}$ IV bolus. The intravenous cannula was flushed with 0.9% saline (grey diamonds) to remove compounds in the tubing. The overshoot in HR following adenosine applications is likely the result of the baroreflex. Insets are expanded HR and blood pressure responses to adenosine (black trace, boxed region in **A** and **B**) and BnOCPA (blue trace and boxed region in **A** and **B**). Scale bars measure: HR, 200 BPM and 6 s; blood pressure, 40 mm Hg and 6 s. **(C, D)**, Summary data for 4 experiments. Data from each rat is shown as a different symbol. Means (± SEM, light grey bars) are connected to indicate the sequential nature of treatments across the four preparations. One-way RM ANOVA for: **(C)**, HR, Greenhouse-Geisser corrected $F(2.33, 7.00) = 68.27$, $P = 2.07 \times 10^{-5}$; **(D)**, mean arterial blood pressure (MAP), Greenhouse-Geisser corrected $F(1.84, 5.52) = 10.51$, $P = 0.014$; with the following Bonferroni post hoc comparisons: The resting HR of 432 ± 21 BPM was significantly reduced to 147 ± 12 BPM (~66 %, $P = 2.76 \times 10^{-11}$) by adenosine. BnOCPA had no significant effect on HR (~6%, 442 ± 20 vs 416 ± 21 BPM; P = 1) but prevented the bradycardic effects of adenosine ($P = 2.71 \times 10^{-9}$ vs adenosine) when co-injected (mean change 51 ± 4 BPM; ~12 %; P = 0.67). CPA significantly decreased HR (from 408 ± 17 to 207 ± 29 BPM; ~50 %, $P = 1.85 \times 10^{-8}$), a decrease that was not significantly different to the effect of adenosine (P = 0.12), but was significantly different to the effect of both BnOCPA ($P = 9.00 \times 10^{-9}$) and adenosine in the presence of BnOCPA ($P = 6.69 \times 10^{-7}$). The resting MAP (86 ± 9 mm Hg) was significantly reduced by adenosine (~47 %, 46 ± 4 mm Hg; P = 0.001). BnOCPA had no significant effect on its own on MAP (88 ± 11 vs 85 ± 13 mm Hg; P = 1) and did not prevent adenosine in lowering MAP to a value similar to adenosine on its own (51 ± 4 mm Hg; P = 1 vs adenosine; P = 0.012 vs BnOCPA alone). CPA significantly decreased MAP (from 83 ± 8 to 51 ± 5 mm Hg; P = 0.017), a decrease that was not significantly different to the effect of adenosine in the

absence or presence of BnOCPA (P = 1 for both). ns, not significant; **, P < 0.02; ***, P < 0.001; ****, P < 0.0001.

Fig. 6 BnOCPA is a potent analgesic without causing respiratory depression

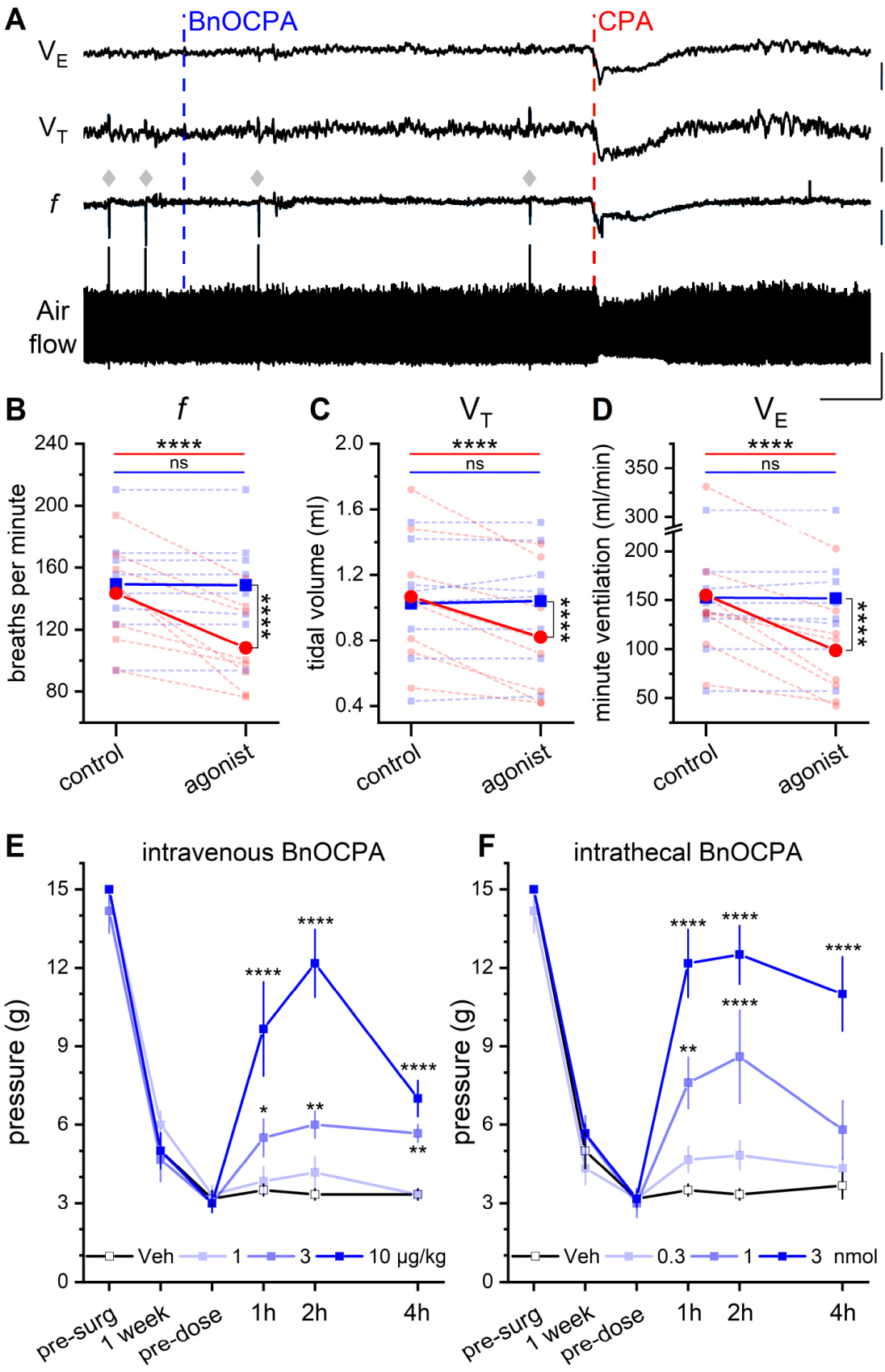

Fig. 6 BnOCPA is a potent analgesic without causing respiratory depression

(A), examples of tracheal airflow, respiratory frequency (*f*), tidal volume (V_T) and minute ventilation (V_E) from a single urethane-anaesthetised, spontaneously breathing rat showing the lack of effect of BnOCPA on respiration and the respiratory depression caused by CPA. BnOCPA and CPA were given as a 350 µL·kg^{-1} IV bolus at the times indicated by the vertical broken lines (BnOCPA, 8.3 ug/kg, blue; CPA, 6.3 µg·kg^{-1}, red). Grey diamonds indicate spontaneous sighs. Scale bars measure: 180 s and: airflow, 0.5 mL; *f*, 50 breaths per minute (BrPM); V_T, 0.25 mL; V_E, 50 mL/min. **(B, C, D),** Summary data for 8 anaesthetised rats. Data from each rat is shown before and after the injection of BnOCPA (blue squares and broken lines) and CPA (red circles and broken lines) together with the mean value for all animals (solid lines) for *f*, V_T and V_E, respectively. One-way RM ANOVA: For: **B**, *f*, Greenhouse-Geisser corrected F(1.20, 8.38) = 30.4, P = 3.48 x 10^{-4}; **C**, V_T, F(3, 21) = 15.9, P = 1.25 x 10^{-5}, and **D**, V_E, Greenhouse-Geisser corrected F(1.19, 8.34) = 15.77, P = 0.003, with the following Bonferroni post hoc comparisons: Following BnOCPA, *f* (149 ± 12 BrPM), V_T (1.0 ± 0.1 mL), and V_E (152 ± 26 ml/min) were not altered (P = 1) compared to resting values *f* (149 ± 12 BPM), V_T (1.0 ± 0.1 mL), and V_E (152 ± 26). In contrast to CPA, which reduced *f* (108 ± 10 BrPM), V_T (0.8 ± 0.1 mL), and V_E (99 ± 19 ml/min) compared to resting values *f* (143 ± 11 BrPM; p = 4.05 x 10^{-6}), V_T (1.1 ± 0.1 mL; P = 2.58 x10^{-5}), and V_E (155 ± 28; P = 5.52 x 10^{-5}). Whilst the control resting values before administration of BnOCPA and CPA were not different to one another (P = 1). The effects of CPA were significantly greater than BnOCPA for *f* (P = 4.48 x 10^{-7}), V_T (P = 1.15 x10^{-4}), and V_E (P = 1.16 x10^{-4}). Horizontal significance indicators above the data show differences between resting values and following IV administration of either BnOCPA (blue line) or CPA (red line). Vertical significance indicators show differences between the effects of BnOCPA and CPA. **(E, F)**, BnOCPA alleviates mechanical allodynia in a spinal nerve ligation (Chung) model of neuropathic pain when administered via an intravenous (IV; **E**) or intrathecal (IT; **F**) route. Prior to surgery (pre-surg) animals had similar sensitivity to tactile stimulation as assessed by Von Frey hair stimulation. Spinal nerve ligation subsequently caused hypersensitivity to touch (mechanical allodynia) as evidenced by the

reduction in the tactile pressure necessary to elicit paw withdrawal (paw withdrawal threshold; PWT) at 1 week after surgery. PWT reaches a similar nadir across all groups prior to vehicle or BnOCPA infusion (pre-dose). Administration of BnOCPA significantly increased PWT in the limb ipsilateral to the site of injury, in a dose-dependent manner (one-way ANOVA (pre-dose, 1, 2 and 4 hrs) for IV BnOCPA: $F(3,80) = 37.3$, $P = 3.44 \times 10^{-15}$; for IT BnOCPA $(3,76) = 47.0$, $P = 0$). Fisher LSD post-hoc comparisons showed significant differences at: IV 3 ug/kg at 1, 2 and 4 hrs, $P = 0.044$, 0.008 and 0.019, respectively, and 10 ug/kg at 1, 2 and 4 hrs, $P = 1.37 \times 10^{-8}$, 6.81×10^{-14} and 3.23×10^{-4}, respectively; IT 1 nmol at 1 and 2 hrs, $P = 0.001$ and 4.16×10^{-5}, respectively, and 10 nmol at 1, 2 and 4 hrs, $P = 9.52 \times 10^{-11}$, 1.42×10^{-11} and 1.41×10^{-8}, respectively. Averaged data (n = 6 per treatment, except for 1 nmol BnOCPA, n = 5) is presented as mean ± SEM. ns, not significant; ∗, $P < 0.05$; ∗∗, $P < 0.02$; ∗∗∗, $P < 0.001$; ∗∗∗∗, $P < 0.0001$.